ACS APPLIED MATERIALS & INTERFACES

RESEARCH ARTICLE

www.acsami.org

# Recyclable SERS Substrates Based on Au-Coated ZnO Nanorods

Godhuli Sinha, Laura E. Depero, and Ivano Alessandri*

INSTM and Chemistry for Technologies Laboratory, University of Brescia, via Branze 38, 25123 Brescia, Italy

Supporting Information

**ABSTRACT:** Vertically aligned Au-coated ZnO nanorods (Au-ZnO NRs) were investigated as cheap, efficient and recyclable SERS-active substrates. The ZnO NRs were prepared through a simple, low-temperature hydrothermal route and made SERS-active through deposition of gold nanoislands by sputtering at room temperature. Optimized samples were able to detect methylene blue over a wide range of low concentrations (from $1 \times 10^{-4}$ to $1 \times 10^{-12}$ M), with good reproducibility. The photocatalytic properties of Au-ZnO NRs were exploited to recycle these substrates through UV-assisted cleaning. The experimental results showed that these substrates are characterized by high reproducibility and long shelf life, which make them promising as SERS platforms for multiple detection of different molecular species.

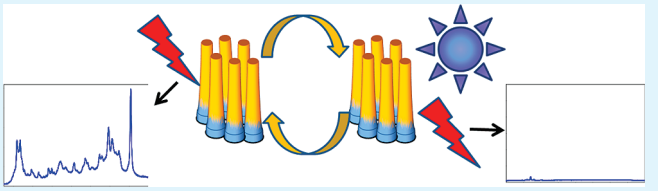

**KEYWORDS:** ZnO nanorods, SERS, SERS substrates, photodegradation, organic pollutants

## 1. INTRODUCTION

Surface-enhanced Raman scattering (SERS) is intensively investigated since it provides a powerful tool for ultrasensitive vibrational spectroscopy, which can lead to major breakthroughs in a number of disciplines, including analytical chemistry, physics, medicine, and life science.[1−4] SERS is due to the surface plasmon-polariton near field generated by interaction of a laser source with a SERS-active substrate. The efficient coupling of such a plasmon-induced near field with vibrational modes of either molecules or crystals adsorbed on the SERS-active substrate can allow to enhance the Raman cross section of the adsorbates by several order of magnitude. Thus, Raman sensitivity can be strongly boosted and, in some cases, extended to the level of single molecule detection.[5,6] Since substrates play a key role in SERS experiments, in many cases they represent a critical bottleneck for developing SERS-based platforms for different applications.[7] In this regard, SERS substrates should meet manifold requirements that sometimes need to find a convenient trade-off with each other. In general SERS substrates are achieved by metallic (in particular Au, Ag, Cu as their surface plasmon resonance falls in the visible region) nanoparticles or nanostructures with different shapes and architectures, prepared through either chemical or physical routes.[8−11] Recently, nanostructures such as nanorods and nanowires have been proposed as promising SERS substrates. For example, silicon nanowires were studied for ultrasensitive Raman analyses,[12] as well as for tip-enhanced Raman spectroscopy (TERS), where they can play both as probes and substrates.[13] In all of these cases, SERS activity is due to the presence of metal nanoparticles, which can be introduced directly as seeds that promote the growth of the nanowires (e.g., Au) and/or deposited by different routes.[14] The dielectric−core/metallic−shell geometry can offer unique advantages for SERS, as it allows concentrating the scattering electromagnetic field at the metal surface.[15] However, most of the approaches used so far are characterized by complicated and expensive preparation steps, or by major flaws in stability and reproducibility. For example, Si nanowires are usually grown through a high-temperature vapor−liquid−solid route, which is quite expensive.[13] Ag nanoparticles are extremely efficient in enhancing the Raman scattering, but they are easily oxidized, so that the substrate lifetime is quite limited. Au nanoparticles are stable against oxidation, but they are often coated with chemical species to control aggregation and ensure their mechanical stability. These protective capping layers may prevent the adsorption of dye molecules on their surfaces or introduce unwanted extra signals in the Raman spectrum. On the other hand, electrochemical roughening does not allow for a fine control of the shape and organization of nanoparticles. Moreover, in general all of these Raman substrates cannot be easily reused. This is a serious drawback not only from the economical standpoint, but also for reproducibility. In fact, one of the most critical issues associated with the application of SERS as a routine-technique is that enhancement factors can vary from one substrate to another, and from different regions of the same substrate. Nanolithographic techniques can greatly increase reproducibility, but at the expense of signal enhancement and economical viability. In this case, the decrease of Raman intensity is ultimately due to the fact that the electromagnetic field is strongly enhanced when the gap between metallic nanoparticles junctions ranges from 1 to 2 nm (the so-called Raman hot spots), whereas the resolution limit of conventional lithographic techniques is ∼10 nm.[16] For these reasons, in recent years, many research efforts have been focused on preparing recyclable SERS substrates.[17−20]

In this paper, we present SERS-active substrates that can be repeatedly used in Raman experiments without losing

Received: April 5, 2011
Accepted: June 2, 2011
Published: June 02, 2011





dx.doi.org/10.1021/am200396n | ACS Appl. Mater. Interfaces 2011, 3, 2557–2563

their sensitivity. These substrates are based on ZnO nanorods (ZnO NRs) grown through a simple, low-temperature hydrothermal route. A thin layer of gold deposited by room temperature (r.t.) sputtering provided SERS activity to the ZnO NRs. Au was chosen in view of its versatile surface chemistry, which comes along with low fluorescence and excellent resistance against oxidation. These properties make these substrates suitable for further functionalization, extending their application to biodiagnostics and nanobiotechnology. Moreover, as it has been shown by both literature[21,22] and our previous works,[23,24] r.t. sputtering is a very useful tool to generate SERS-active uncapped Au nanoislands, as it is a very simple, low-cost technique. ZnO has been recently exploited as a potential candidate for fabrication of SERS substrates since its high refractive index promotes strong light confinement, which can further contribute to increase the SERS effect.[15,25−28] In addition, Lombardi and co-workers observed SERS spectra of aminothiophenols adsorbed in Au−ZnO nanoparticles as a result of the ZnO-assisted enhanced charge-transfer from the metal to the molecule.[29] In the present case, we exploited the photocatalytic properties of ZnO to promote the UV light-induced degradation of the analytes so that, after SERS analysis, the substrates can be cleaned and reused for other Raman measurements. Detection limits, reproducibility, and reprocessing of the SERS substrates were investigated through different series of Raman experiments in order to check the reliability of this approach.

## 2. EXPERIMENTAL SECTION

**2.1. Preparation and Structural and Microstructural Characterization of the Sers-Active Substrates.** The ZnO nanorods (ZnO NRs) were hydrothermally grown starting from ZnO seed layers, which had been deposited onto cleaned Si wafers by atomic layer deposition (ALD). To prepare the seed layers Diethylzinc (DEZ, Sigma-Aldrich) and deionized water (Milli-Q grade) were used as precursors of zinc and oxygen, respectively. The deposition was carried out in a Savannah 100 ALD flow reactor (Cambridge Nanotech Inc., MA) in continuous mode at a growth temperature of 90 °C and the operating pressure was maintained at 0.8 Torr with a total gas flow rate of 20 s.ccm The processing cycle consisted of alternating DEZ and water pulses (for 0.1 and 0.015 s, respectively), each one followed by nitrogen purging for 10 s. The deposition rate was 0.13 nm per cycle and seed layers with nominal thickness varying from 10 to 50 nm were used in these sets of experiments. All of these data were evaluated by X-ray reflectivity (XRR, Bruker D8 diffractometer).

After seeding, hydrothermal growth of ZnO NRs was performed by suspending the substrates upside-down in a thermal container. 0.02 M solution of Zinc nitrate hexahydrate ($Zn(NO_3)_2 \cdot 6H_2O$) and 0.04 M solution of hexamethylenetetramine (HMT) in distilled water ($H_2O$) were prepared and equal volume aliquots of each solution were mixed together. All the chemicals were analytical grade and used without further purification. Before introducing the substrate into the growth solution, the precursor solution was maintained in a laboratory hydrothermal chamber at 90 °C for 1 h to stabilize the growth temperature. The ZnO-seeded Si wafers were inserted into the precursor solution at an acute angle and maintained at 90 °C for 6 h. The as-grown samples were rinsed in deionized water, and then dried in air.

The ZnO NRs were coated with gold by sputtering (K550-SEM sputter coater) at room temperature. Before deposition, the pressure in the vacuum chamber was decreased down to $7 \times 10^{-2}$ mbar. We used different deposition times, between 20 and 60 s with a current of 25 mA.

XRD data were acquired by an X'pert Pro Panalytical X-ray diffractometer (radiation source: Cu $K_\alpha$, current: 40 mA, voltage: 40 kV). Scanning electron microscope images were acquired by a LEO 1521 high resolution instrument equipped with field emission gun and in-lens secondary electrons detector.

**2.2. UV−Vis Characterization of the Substrates and SERS Experiments.** The absorbance spectra of Au-coated- and bare ZnO NRs redispersed in isopropanol were monitored by an Ocean Optics QE65000 fiber-optic UV−vis spectrophotometer. Methylene Blue (MB, $C_{16}H_{18}N_3SCl$), which served as molecular probe for Raman experiment, was purchased from Sigma-Aldrich and used without further purification. The diluted solutions with concentration varying from $1 \times 10^{-4}$ to $1 \times 10^{-12}$ M were prepared in miliQ water. The SERS spectra of the MB dip-coated substrates were obtained with High Resolution Horiba Jobin-Yvon Labram-800 spectrophotometer equipped with a confocal microscope. The excitation source was 632.8 nm line from He−Ne laser, which was focused onto the sample with 100× (Numerical Aperture: 0.90) objective, with acquisition time of 40 s.

**2.3. Photocatalytic Measurements and Cleaning Cycles.** The photocatalytic self-degradation experiment were performed by irradiating a vessel containing a $1 \times 10^{-5}$ M aqueous solution of MB with a Philips UV lamp, which emits in the range 340−410 nm with a maximum at 365 nm. The distance between the lamp and the vessel was 1 cm. The photocatalytic activity of ZnO NRs and Au-ZnO NRs was tested using the same experimental setup, by fixing the substrates at the vessel bottom. The concentration of MB was determined by monitoring the absorbance of the main MB band (663 nm) as a function of irradiation time.[30]

The UV-assisted substrate cleaning cycles consisted of the following steps: after SERS characterization of the MB adsorbed onto the optimized Au-ZnO NRs, these substrates were wetted with a Milli-Q water drop and UV irradiated at different times (15 and 30 min) under the conditions reported above. The irradiated substrates were thoroughly rinsed in deionized water, dried at room temperature and reused for Raman detection experiments. Each cycle was repeated 10 times.

## 3. RESULTS AND DISCUSSION

The ZnO NRs to be used as SERS-active substrates were grown onto planar Si wafers through a modified HMT-assisted hydrothermal route at 90 °C. Literature has demonstrated that HMT decomposition promotes the growth of 1D nanostructures.[31−34] However, unlike pure hydrothermal methods, where a fine control of the crystal orientation is often severely limited by several factors (pH, time, temperature..) in the present case we promoted the growth of NRs through a ZnO seeding layer deposited by ALD. This preliminary process allows the uniform generation of densely distributed ZnO islands, whose size can be tailored by changing the number of ALD cycles.[35]

Figure 1 shows X-ray diffraction (XRD) patterns of ZnO NRs hydrothermally grown from seeds achieved upon 77 (sample I) and 385 (sample II) ALD cycles, respectively. Whereas (100) is the most intense peak in bulk, isotropic wurtzite samples (ZnO powders, JCPDS: 36−1451), in the present case we observed that the strongest reflections were (100) and (002) for samples I and II, respectively. Thus the NRs exhibit preferred orientation, and the crystal alignment switches from parallel (sample I) to perpendicular (sample II) to the substrate, depending on the number of ALD cycles. Few ALD cycles give results very similar to those obtained for ZnO NRs that have been grown without any seeding layer (see the Supporting Information). For the present studies we are mainly interested in growing vertically aligned ZnO NRs, because this type of orientation allows us to get rid of the contributions to the SERS effect which originates from cross-junctions between tilted and/or horizontally oriented

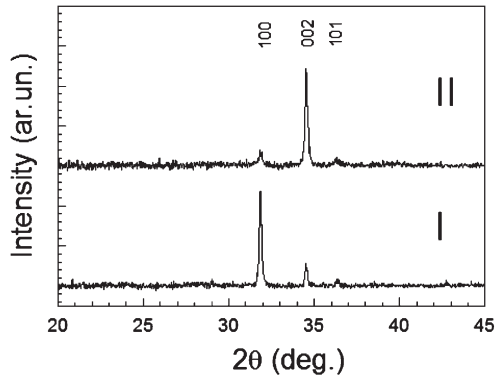


**Figure 1.** XRD patterns of ZnO NRs hydrothermally grown from ZnO seeds deposited through 77 (sample **I**) and 385 (sample **II**) ALD cycles.

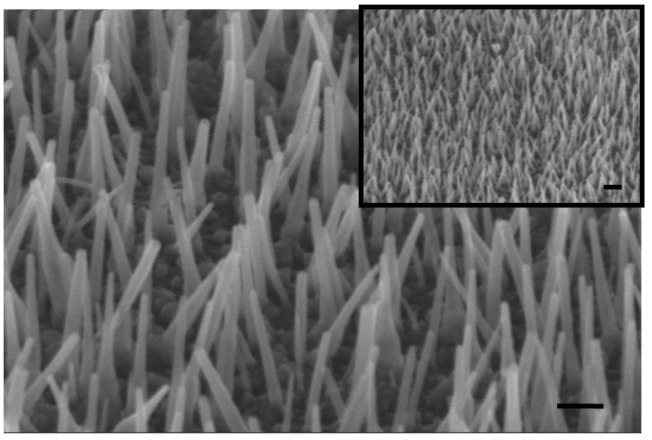

**Figure 2.** SEM of vertically aligned ZnO NRs hydrothermally grown from ZnO seeds. A lower magnification view is shown in the inset. Scale bars: 100 nm.

NRs. In fact, although these contributions can strongly increase the SERS effect, they are very difficult to predict and represent a major source of irreproducibility. We observed that best results were obtained for 385 cycles, which correspond to an ideal, continuous ZnO layer with a nominal thickness of 50 nm. The SEM images of this sample batch, which was used for the following experiments, confirmed the vertical alignment of the NRs, which are uniformly and densely distributed all over the substrate (Figure 2). The length of the NRs ranges from 300 to 400 nm and their width is between 30 and 40 nm, so that the aspect ratio is ~10. To provide SERS activity, these NRs were coated with gold by sputtering at room temperature. Different deposition times (20, 30, and 60 s) were tested. UV−vis absorption spectra, obtained upon collection and redispersion of the NRs in isopropanol are shown in Figure 3a. The absorption edge at 368 nm observed in all the samples corresponds to the bulk value (3.37 eV) of the ZnO band gap. The as-prepared ZnO NRs are transparent in the visible region, as expected. Upon sputtering for 20 s, a broad plasmon band, centered at ~540 nm appeared, indicating the formation of Au nanoparticles onto ZnO nanorods (sample A). This band shifted to about 580 nm and became stronger by increasing deposition time up to 30 s (sample B). This trend is commonly observed in most of the systems containing Au nanoparticles. In general, red shifting and broadening of the plasmon resonance is due to the nanoparticles

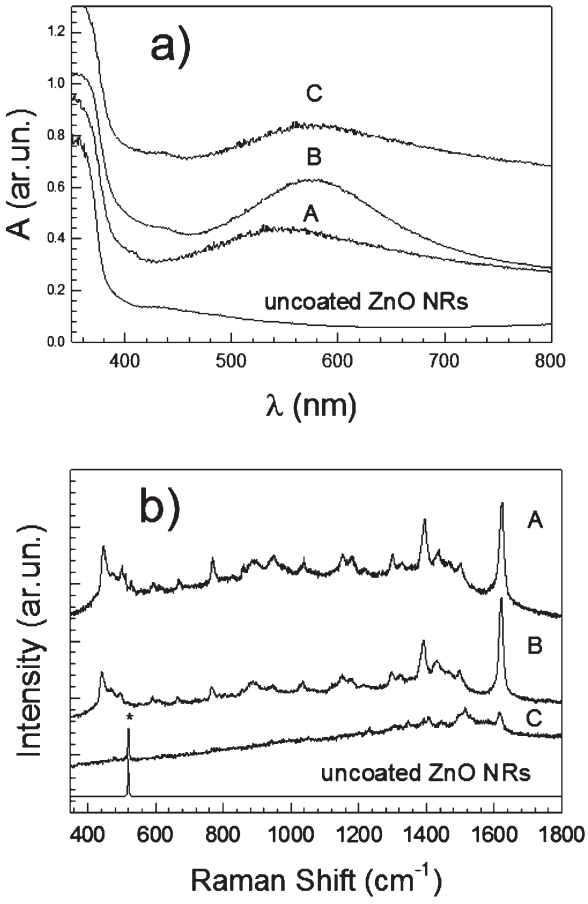


**Figure 3.** (a) UV−vis spectra of ZnO NRs coated with Au at different r.t. sputtering time: 20 s (sample A), 30 s (sample B), and 60 s (sample C). The spectrum of uncoated ZnO NRs was reported as a reference. (b) Raman spectra of a $1 \times 10^{-6}$ M solution of MB acquired from A, B, and C substrates types. The Raman spectrum of a $1 \times 10^{-6}$ M MB solution adsorbed onto uncoated ZnO NR substrates was shown for comparison. The peak of the Si wafer is indicated by an asterisk.

aggregation, which results in stronger dipole−dipole interactions. Upon further incrementing deposition time to 60 s or more, the plasmon band was progressively weakened and broadened, as usually observed for continuous films (sample C). The Raman activity of these three substrates was evaluated by detecting the spectra of a $1 \times 10^{-6}$ M solution of MB, one of the most widely used organic dyes. (Figure 3b) MB is an useful probe for our purposes, not only as it represents a good model system for evaluating detection and possible degradation of heterocyclic aromatic dyes, but also because it has been previously used as a molecular probe for other SERS-active supports, such as Au nanorods,[36] so that it may provide an indirect evaluation of the substrate performances. In the visible part of the spectral region MB exhibits a strong absorption band, which is split into two main peaks, at ~610 and ~660 nm, corresponding to dimeric and monomeric species, respectively.[36] Because the wavelength of the He−Ne laser source ($\lambda$ = 632.8 nm) used for excitation matches the MB absorption band, the Raman measurements were carried out under resonant conditions. During spectra acquisition the power of the laser source was attenuated to 0.5 mW to avoid any side-phenomena, such as photobleaching or photodesorption. This precaution is mandatory as clusters of Au

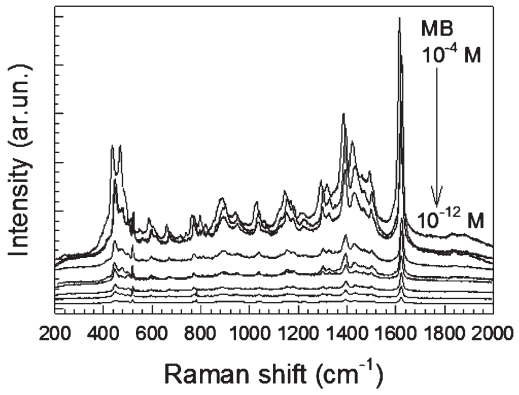


**Figure 4.** Raman spectra of MB solutions at nine different concentration ($1 \times 10^{-4}$ to $1 \times 10^{-12}$ M). A comparison between SERS and non-SERS spectra is reported in the Supporting Information.

nanoparticles can develop strong heating effects upon laser irradiation.[37−39]

Under normal (non-SERS) conditions, MB cannot be detected at this concentration, as displayed by the Raman spectra of MB adsorbed onto bare ZnO. On the other hand, Raman signals can be observed in all of the three gold-coated supports. (Figure 3b) Each one of the Raman spectra shown in this figure are the average of spectra acquired over ten different position of the substrate. The spectra showed all the Raman-active vibrational features of MB, which is characterized by strong signals around 445, 475, 1147,1382, 1422 $cm^{-1}$ (C−N−C skeletal bending), 1494 and 1618 $cm^{-1}$ (C−C ring stretching).[36]

Substrates A and B exhibited strong Raman signals, whereas substrate C only gave a quite limited contribution to MB detection. This result could have been partially expected on the basis of UV−vis data, which showed the maximum surface plasmon resonance for sample B and the minimum for sample C. However, although UV−vis spectra allow to evaluate the extent of surface plasmon resonance, they provide only a rough indication on matching between incident laser and surface plasmon resonance. In fact, this information is averaged all over the sample, but it does not account for local hot spots, which are the major contributors to the enhancement of the Raman signal. This can be observed in sample A, which showed a very good Raman spectrum, in spite of the wavelength mismatch between its surface plasmon band (535 nm) and the exciting source (632.8 nm). Likewise, the surface plasmon resonance of sample B is closer, but not enough for exactly matching the wavelength of the laser. Since the ZnO NRs used as SERS- active substrates were vertically aligned, hot spots originated from junctions between crossing NRs should be minimized. Thus, in the present case, the major source of hot spots must be sought in the morphology of the gold coatings. Room-temperature sputtering promotes the nucleation of a large number of gold islands (see the Supporting Information), which eventually evolve to continuous thin layers in thicker coatings. The multiple gaps between adjacent islands, which are, in many cases, well below 5 nm, can yield a strong intensification of the electromagnetic field, giving rise to enhanced Raman scattering. This hypothesis agrees with a number of similar cases reported in literature and can qualitatively explain the slight increase of the Raman enhancement on passing from sample A to B and the subsequent decrease observed in thicker samples. These experimental results allowed to sort out a series of optimized substrates (samples B), which have been used for the following experiments. The detection capabilities of these substrates were evaluated with MB solutions over a wide range of concentration ($1 \times 10^{-4}$ to $1 \times 10^{-12}$ M, Figure 4). Thanks to the enhanced Raman scattering promoted by gold nanoislands, these substrates are able to extend their detection limit by 8 orders of magnitude with respect to the analogous bare ZnO NRs (see the Supporting Information). A reliable calculation of the enhancement factor (EF) through the general formula $EF = (I_{SERS}/N_{Surf})/(I_{RS}/N_{Vol})$ (where $I_{SERS}$ and $I_{RS}$ are the Raman signals under SERS and normal conditions, respectively, $N_{Vol}$ is the average number of molecules in the Raman (non-SERS) scattering volume and $N_{Surf}$ is the average number of adsorbed molecules in the SERS scattering volume) cannot be performed due the absence of data about the number of MB molecules which are actually adsorbed onto these Au−ZnO NRs. In fact, as exhaustively demonstrated by Le Ru et al., this formula is limited by some constraints and affected by major flaws which can be severely amplified in the case of substrates characterized by a complex morphology, like nanorods, nanowires and 3D architectures.[40] However, the simple evaluation of the intensity ratios between the main peaks of SERS and non-SERS spectra of MB showed that SERS signals are more than 20 times stronger than the corresponding non-SERS. All these observations can be qualitatively explained by considering that the Raman cross sections of molecules involved in a SERS process (a SERRS process, in the present case) are, in general, of the order of $1 \times 10^{-15}$ to $1 \times 10^{-16}$ $cm^2$, whereas those associated with the simple resonant Raman scattering are limited to $1 \times 10^{-24}$ $cm^2$.[1,2] On the basis of our previous results, we can observe that the SERS performances of the Au−ZnO NRs substrates are comparable to those exhibited by gold nanorods with the same molecular probe.[36] However, the fabrication of Au−ZnO NRs is easier and the SERS results much more reproducible.

As discussed above, one of the main advantages of Au-coated ZnO NRs in comparison to other SERS supports is their potential recyclability. In this case, the photocatalytic activity of ZnO NRs could be exploited to remove the molecules under analysis and make the substrates ready for a new detection cycle. Figure 5a shows the absorbance of a $1 \times 10^{-5}$ M solution of MB (pH 6.9) upon UV irradiation. The characteristic absorption bands retained their full intensity even after 3 h, so that MB can be considered stable against UV-induced self-degradation. On the other hand, MB is progressively degraded in presence of both ZnO and Au−ZnO NRs (Figures 5b,c). The photodegradation of MB is generally assumed to proceed through a Langmuir−Hinshelwood mechanism ($\ln C/C_0 = kt$, where $C$ is the MB concentration as a function of photodegradation time, $C_0$ the initial concentration and k the apparent reaction-rate constant).[41] Monitoring the change of absorbance of the main peak at 663 nm as a function of irradiation time (Figure 5d), we can observe that the Au-coated ZnO NRs are more efficient than the uncoated ZnO NRs ($k$ = 0.021 and 0.012 $min^{-1}$, respectively). Analogous results were achieved for photodegradation of other dyes, such as Rhodamine B (see the Supporting Information). Likewise, other semiconductor oxides, the general mechanism of photocatalysis via ZnO NRs is based on UV light-induced generation of electron−hole pairs, which react with both oxygen and water molecules to yield strongly oxidizing radical species, which in turn promote the oxidation of organic substrates (see the Supporting Information). Enhancements of photocatalytic efficiency due to the introduction of Au nanoparticles were

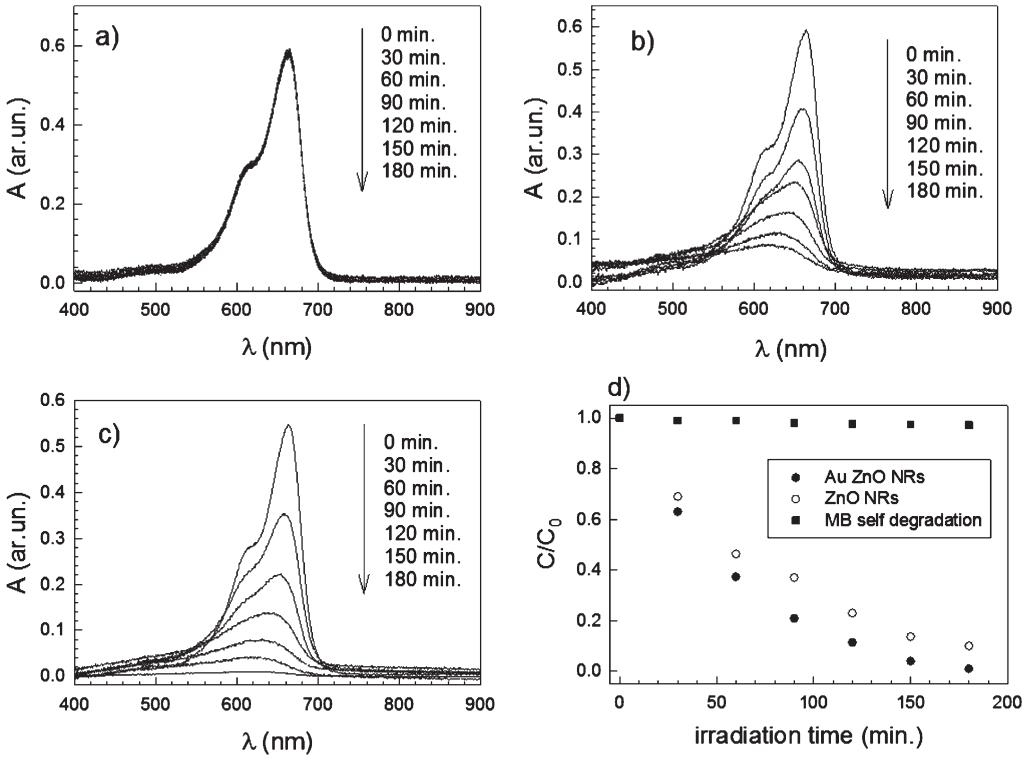


**Figure 5.** UV-induced photodegradation of MB as a function of irradiation time: Visible spectra showing (a) MB self-degradation, (b) MB degradation promoted by ZnO NRs, and (c) MB degradation promoted by Au-ZnO NRs. (d) $C/C_o$ vs. irradiation time. See the text for details.

reported in literature also for other semiconducting photocatalysts, such as $TiO_2$.[42,43] In these cases, the Au-semiconductor interface allows for an efficient separation of charges, which triggers the redox processes involved in photodegradation. On the other hand, at too high concentrations, Au nanoparticles can also play as recombination centers, with a consequent decrease of the overall photoactivity.[42] At the same time, we have previously demonstrated that thicker Au coatings can be detrimental also for the SERS activity. Being both photocatalytic- and SERS-active, these Au-ZnO NRs can be exploited as optimized substrates for multiple using. The SERS substrates can be cleaned in several ways. For example, after Raman analysis, the substrates were coated with a drop of deionized water (Milli-Q grade), UV-irradiated and then repeatedly rinsed in deionized water. Figure 6a shows the Raman spectra of MB adsorbed on the substrate before and after cleaning. The spectra were mediated over 20 different spatial positions. After 15 min the MB signal is very weak and it completely vanishes after 30 min. The photodegradation occurred faster compared to the trend we previously observed for the MB "bulk" solutions, since the actual amount of the MB adsorbed onto the substrates is very low. The signal is fully recovered after further soaking of the substrate into the MB solution, indicating that both Au and ZnO preserve their functionality. This cycle was repeated ten times, giving reproducible results (Figure 6b) and full SERS activity was kept upon storage in air for several months.

In addition to its obvious economical benefit, recyclability also provides the unique opportunity of analyzing different molecules with a common SERS platform. This aspect could become a key factor in view of evaluating the Raman cross sections of different molecular probes and to study charge transfer processes at the semiconductor-metal-molecule interfaces.

These substrates offer important advantages in comparison to other recyclable systems based on titania nanotubes, in which the best photocatalytic performances were obtained at the expense of the optimal SERS activity and viceversa.[18] Moreover, the direct use of ZnO NRs, which usually serve as sacrificial templates and need to be dissolved during the growth of titania nanotubes,[18] allows to skip most of the fabrication steps, making the preparation of recyclable SERS substrates very easy. The Au-NRs can be suitable for SERS analysis of a variety of molecules, including organic pollutants and biochemically active species, provided that they could be efficiently removed by cleaning cycles. In this regard, we could expect good results for organic dyes or thiolated bioconjugates (the latter can be removed by ozone-UV cleaning) whereas removal of either proteins or other very stable/"sticky" species could be much more difficult. On the other hand, these substrates cannot be used in very acidic or basic conditions, due to ZnO dissolution. New procedures, based on protecting conformal layers of alumina deposited by ALD[44,45] are currently under investigation in order to stabilize the ZnO NRs. Since chemical stability could go along with the thermal one, novel strategies relying on rapid thermal degradation of the analyzed molecules could be concurrently developed. In perspective, very fast degradations could be also achieved using ozone-UV cleaners at moderate temperatures, whereas plasmonic-assisted photodegradation could be exploited to remove the organic molecules under visible irradiation. All of these alternative strategies will be the object of further investigations.

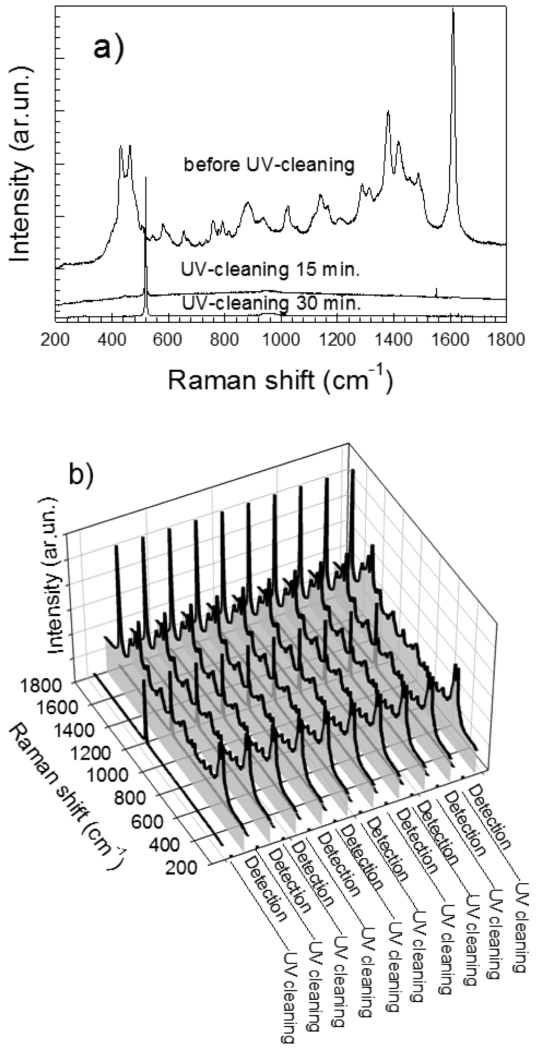


**Figure 6.** (a) Raman spectra of MB solution ($1 \times 10^{-4}$ M) adsorbed onto Au-NRs before and after UV-cleaning. (b) Raman spectra of ten adsorption/UV-cleaning cycles. Each cycle consists of adsorption of MB solution followed by UV irradiation for 30 min (see the text for details). The graphs shows the Raman spectra before and after cleaning. Each Raman spectrum was averaged over 20 different spatial positions.

## 4. CONCLUSION

We experimentally demonstrated that Au-coated ZnO NRs can be used as efficient, cheap and recyclable SERS-active substrates. The vertically aligned ZnO NRs were prepared through a simple, low-temperature hydrothermal route and made SERS-active through deposition of gold nanoislands by sputtering at room temperature. After individuation of the critical parameters, the fabrication was optimized in order to yield substrates developing both strong SERS activity and efficient photodegradation. 30 s-Au coated ZnO NRs were able to detect MB molecular probes down to $1 \times 10^{-12}$ M with good reproducibility. These substrates were also successfully tested in several UV-assisted cleaning cycles. In particular, MB has been demonstrated to undergo rapid photodegradation and removal after each cleaning cycle. At the same time, the SERS response before each cleaning cycle was highly reproducible and the substrates were characterized by a long shelf life. All the above-mentioned features make these substrates quite promising to exploit SERS and related effects for routine Raman analyses.

## ■ ASSOCIATED CONTENT

**Supporting Information.** SEM images of Au nanoislands deposited by sputtering, comparison between SERS and non-SERS Raman spectra of MB, photodegradation of Rhodamine B by Au-coated and uncoated ZnO NRs. This material is available free of charge via the Internet at: http://pubs.acs.org.

## ■ AUTHOR INFORMATION

### Corresponding Author

*Phone: +39 030 3715667. Fax: +30 030 3702448. E-mail: ivano.alessandri@ing.unibs.it.

## ■ ACKNOWLEDGMENT

This work has been supported by Fondazione Cariplo. G. S. thanks the Italian Ministry of the Education, University and Scientific Research (MIUR) for a grant in the framework of a cooperation for young Indian researchers. Dr. Matteo Ferroni is gratefully acknowledged for assistance in SEM analysis. We thank Dr. Laura Borgese for assistance in ALD.

## ■ REFERENCES

(1) Aroca, R. *Surface-Enhanced Raman Spectroscopy*; Wiley: New York, 2006.
(2) Le Ru, E. C.; Etchegoin, P. G. *Principles of Surface-Enhanced Raman Spectroscopy and Related Plasmonic Effects*; Elsevier: Amsterdam, 2009.
(3) Anker, J. N.; Hall, W. P.; Lyandres, O.; Shah, N. C.; Zhao, J.; Van Duyne, R. P. *Nat. Mater.* **2008**, *7*, 442–453.
(4) Moskovits, M. *J. Raman Spectrosc.* **2005**, *36*, 485–496.
(5) Kneipp, K.; Wang, Y.; Kneipp, H.; Perelman, L. T.; Itzkan, I.; Dasari, R. R.; Feld, M. S. *Phys. Rev. Lett.* **1997**, *78*, 1667–1670.
(6) Nie, S. M.; Emory, S. R. *Science* **1997**, *275*, 1102–1106.
(7) Formo, E. V.; Mahurin, S. M.; Dai, S. *ACS Appl. Mater. Interfaces* **2010**, *2*, 1987–1991.
(8) Banholzer, M. J.; Millstone, J. E.; Qin, L.; Mirkin, C. A. *Chem. Soc. Rev.* **2008**, *37*, 885–897.
(9) Cerf, A.; Molnàr, G.; Vieu, C. *ACS Appl. Mater. Interfaces* **2009**, *1*, 2544–2550.
(10) Ko., H.; Singamaneni, S.; Tsukruk, V. V. *Small* **2008**, *4*, 1576–1599.
(11) Alessandri, I.; Depero, L. E. *ACS Appl. Mater. Interfaces* **2010**, *2*, 594–602.
(12) Galopin, E.; Barbillat, J.; Coffinier, Y.; Szunerits, S.; Patriarche, G.; Boukherroub, R. *ACS Appl. Mater. Interfaces.* **2009**, *1*, 1396–1403.
(13) Becker, M.; Sivakov, V.; Gösele, U.; Stelzner, T.; Gudrun, A.; Reich, H. J.; Hoffmann, S.; Michler, J.; Christiansen, S. H. *Small* **2008**, *4*, 398–404.
(14) Li, D.; Li, D. W.; Li, Y.; Fossey, J. S.; Long, Y. T. *J. Mater. Chem.* **2010**, *20*, 3688–3693.
(15) Qi, H.; Alexson, D.; Glembocki, O.; Prokes, S. M. *Nanotechnology* **2010**, *21*, 085705.
(16) Le Ru, E. C.; Etchegoin, P. G. *J. Chem. Phys.* **2009**, *130*, 181101–3.
(17) Aldeanueva-Potel, P.; Faoucher, E.; Alvarez-Puebla, R. A.; Liz-Marzan, L. M.; Brust, M. *Anal. Chem.* **2009**, *81*, 9233–9238.
(18) Li, X.; Chen, G.; Yang, L.; Jin, Z.; Jinhuai, L. *Adv. Funct. Mater.* **2010**, *20*, 2815–2824.
(19) Choi, J. Y.; Kim, K.; Shin, K. S. *Vib. Spectrosc.* **2010**, *53*, 117–120.
(20) Mahurin, S.; John, J. F.; Sepaniak, M. J.; Dai, S *Appl. Spectrosc.* **2011**, *65*, 417–420.

(21) Maya, L.; Vallet, C. E.; Lee, Y. H. *J. Vac. Sci. Tachnol., A* **1996**, *15*, 238–242.
(22) Merlen, A.; Gadenne, V.; Romann, J.; Chevallier, V.; Patrone, L.; Valmalette, J. C. *Nanotechnology* **2009**, *20*, 215705.
(23) Alessandri, I.; Ferroni, M.; Depero, L. E. *Chem. Phys. Chem.* **2009**, *10*, 1017–1022.
(24) Alessandri, I.; Depero, L. E. *Chemical Commun.* **2009**, *17*, 2359–2361.
(25) Khan, M. A.; Hogan, T. P.; Shanker, B. *J. Raman Spectrosc.* **2009**, *40*, 1539–1545.
(26) Chen, L.; Luo, L.; Chen, Z.; Zhang, M.; Zapien, J. A.; Lee, C. S.; Lee, S. T. *J. Phys. Chem. C* **2010**, *114*, 93–100.
(27) Cheng, C.; Yan, B.; Wong, S. M.; Li, X.; Zhou, W.; Yu, T.; Shen, Z.; Yu, H.; Fan, H. J. *ACS Appl. Mater. Interfaces* **2010**, *2*, 1824–1828.
(28) Wang, Y.; Ruan, W.; Zhang, J.; Yang, B.; Weiqing, X.; Zhao, B.; Lombardi, J. R. *J. Raman Spectrosc.* **2009**, *40*, 1072–1077.
(29) Yang, L.; Ruan, W.; Jiang, X.; Lombardi, J. R. *J. Phys. Chem. C* **2009**, *113*, 117–120.
(30) Alessandri, I.; Zucca, M.; Ferroni, M.; Bontempi, E.; Depero, L. E. *Small* **2009**, *5*, 336–340.
(31) Vayssieres, L. *Adv. Mater.* **2003**, *15*, 464–466.
(32) Gao, X. D.; Li, X. M.; Yu, W. D.; Li, L.; Qiu, J. *Appl. Surf. Sci.* **2007**, *253*, 4060–4065.
(33) Yang, M.; Yin, G.; Huang, Z.; Liao, X.; Kang, Y.; Yao, Y. *Appl. Surf. Sci.* **2008**, *254*, 2917–2921.
(34) Ichikawa, T.; Shiratori, S. *Inorg. Chem.* **2011**, *50*, 999–1004.
(35) Alessandri, I.; Zucca, M.; Ferroni, M.; Bontempi, E.; Depero, L. E. *Crys. Growth. Des.* **2009**, *9*, 1258–1259.
(36) Pal, S.; Depero, L. E.; Alessandri, I. *Nanotechnology* **2010**, *21*, 425701.
(37) Alessandri, I.; Depero, L. E. *Nanotechnology* **2008**, *19*, 305301.
(38) Alessandri, I. *J. Colloid Interface Sci.* **2010**, *351*, 576–579.
(39) Alessandri, I. *Small* **2010**, *6*, 1679–1685.
(40) Le Ru, E. C.; Blackie, E.; Meyer, M.; Etchegoin, P. G. *J. Phys. Chem. C* **2007**, *111*, 13794–13803.
(41) Kitture, R.; Koppikar, S. J.; Kaul-Ghanekar, R.; Kale, S. N. *J. Phys. Chem. Solids* **2011**, *72*, 60–66.
(42) Alessandri, I.; Ferroni, M. *J. Mater. Chem.* **2009**, *19*, 7990–7994.
(43) Subramanian, V.; Wolf, E. E.; Kamat, P. V. *J. Am. Chem. Soc.* **2004**, *126*, 4943–4950.
(44) Whitney, A. V.; Elam, J. W.; Zou, S. L.; Zinovev, A. V.; Stair, P. C.; Schatz, G. C.; vanDuyne, R. P. *J. Phys. Chem. B* **2005**, *109*, 20522–20528.
(45) John, J. F.; Mahurin, S.; Dai, S.; Sepaniak, M. J. *J. Raman Spectrosc.* **2010**, *41*, 4–11.